Reverse Monte Carlo studies of nanoporous carbon from TiC

2005 J. Phys.: Condens. Matter 17 3509

(http://iopscience.iop.org/0953-8984/17/23/004)

INSTITUTE OF PHYSICS PUBLISHING JOURNAL OF PHYSICS: CONDENSED MATTER

J. Phys.: Condens. Matter **17** (2005) 3509–3524 doi:10.1088/0953-8984/17/23/004

Reverse Monte Carlo studies of nanoporous carbon from TiC

Per Zetterström[1], Sigita Urbonaite[2], Fredrik Lindberg[2], Robert G Delaplane[1], Jaan Leis[3] and Gunnar Svensson[2]

[1] The Studsvik Neutron Research Laboratory, Uppsala University, SE-611 82 Nyköping, Sweden
[2] Department of Structural Chemistry, Stockholm University, SE-106 91 Stockholm, Sweden
[3] Tartu Tehnoloogiad Oü, 185 Riaa Street, 51014 Tartu, Estonia

Received 22 December 2004, in final form 20 April 2005
Published 27 May 2005
Online at stacks.iop.org/JPhysCM/17/3509

Abstract

The structures of nanoporous carbon prepared by chlorination of TiC at five different temperatures (700–1100 °C) have been studied by means of reverse Monte Carlo modelling of neutron diffraction data $S(q)$, $0.3 < q < 10.5$ Å^{-1}, using an atomic configuration (8000 atoms) with a density corresponding to 0.62 of graphite. Four different starting models were tested: (i) random atom configuration, (ii) separated graphite sheets and (iii) two defect models created by removing atoms in a graphite structure to obtain the wanted density. To increase the feasibility of the resulting atom configurations, a number of hard and soft constraints were introduced into the software. The hard constraints were (i) a minimum C–C distance of 1.0 Å, (ii) a co-ordination constraint for nearest-neighbour distances of up to 1.6 Å to avoid zero- or single- co-ordinated atoms and (iii) no atoms between 1.7 and 2.1 Å to avoid small unphysical peaks in the radial distribution function. A soft constraint was centred C–C–C angles around 120° with a variance of 6°. The best fit between observed and calculated $S(q)$ was obtained for the defect models. An evaluation of the porosity and surface area corresponding to the atomic configuration showed a significant difference between the 700 and 1000 °C samples and the one prepared at 1100 °C in agreement with HREM and sorption studies.

1. Introduction

Nanoporous solids such as activated carbons are very popular in science and technology due to their wide use in various applications e.g. separation, purification and catalytic processes. There are numerous qualities of activated carbons, depending on the intended application which ranges from removing taste and colour from liquids to more technically advanced applications in batteries, super-capacitors [1] and purification of gases and gas-storage [2, 3]. The performance of these carbons depends on the pore size distribution and in many applications a very narrow one is most desirable. For some years we have been interested in nanocarbons

prepared by chlorination of various carbides [4, 5]. These carbons have been shown to have superior properties in super-capacitors [6] and have been considered for use in technological applications where single-wall nanotubes are currently being tested [7]. Chlorination of metal carbides allows the bulk production of chemically pure nanoporous carbons, which is a necessary demand for many technological processes and applications. Therefore it is important to study how synthetic conditions (e.g. precursor carbide, chlorination conditions and presence of catalytic substances [8]) influence the structure and properties of the resulting carbon.

The study of the atomic structure of amorphous carbon materials is a very complex task, which has concerned an increased interest during recent years. Often a combination of methods is used. X-ray (XRD) and neutron powder diffraction data contain structural information although it is not straightforward to obtain three-dimensional structural models. XRD has been used for many years to obtain information about the crystallinity (the degree of graphitization) of the material. Franklin [9, 10] showed in her pioneering work in the 1950s how to quantify the degree of crystallinity using the half-width of the diffraction peaks. An alternative method to estimate how many graphene monolayers (plate fragments) are joined in coplanar graphite packets is to compare the relative intensity of the 002 (I_{002}) and 100 (I_{100}) reflections [11]. The position of the 002 reflection corresponding to the interlayer distance between the graphitic layers also gives information about the correlation between the layers and thereby also the degree of graphitization [12]. In graphite the interlayer distance is 3.35 Å while in activated carbons it increases up to 3.50 Å, indicating a much weaker interaction between the layers, such as in turbostratic carbon. (However, these parameters are not easily determined in very amorphous materials like those in the present study.)

Structural information concerning the disorder and order of carbons can also be provided from Raman studies. Raman spectra of amorphous carbons contain two broad peaks, G (graphite) and D (disordered) bands typically at 1500–1630 cm^{-1} and around 1360 cm^{-1}, respectively [13]. The relative intensity ratio of these peaks (I_D/I_G) in highly amorphous carbon having graphene plate sizes below 20 Å is correlated with the crystalline size along the basal plane, L_a, according to $I_D/I_G = C \cdot L_a^2$. For nanocrystalline graphite with an L_a above 20 Å a reversal relationship between the intensity ratio and L_a is observed ($I_D/I_G = C(\lambda)/L_a$).

TEM studies clearly show the models based on rigid graphitic plates to be a coarse oversimplification; see e.g. [14]. Today there seems to be some consensus that the graphene fragments in highly amorphous carbons are curved although this curvature varies. However, the exact dimensionality, e.g. whether the fragments are infinite sheets or not, is not completely clarified.

In addition to the quantification of the crystallinity discussed above it is also fairly straightforward to calculate radial-distribution functions (RDFs or $g(r)$), which show the probability of two inter-atomic distances occurring in the specimen, from the structure factor $S(q)$. $S(q)$ is derived from diffraction experiments using electrons [15], x-rays [16] or neutrons [17]. Two methods for obtaining an RDF are direct Fourier transformation of the total structure factor [18] or by indirect modelling, e.g. using a reverse Monte Carlo algorithm in one dimension (MCGR) [19, 20]. However, the co-ordination number (number of atoms surrounding a target atom at a certain distance), which is proportional to the peak area ($4\pi\rho \int r^2 g(r)\,dr$) in $g(r)$, is very sensitive to the correction of the data. The structure factor, $S(q)$, should be placed on an absolute scale. One parameter, which causes surprisingly large difficulties, is the density ρ of highly amorphous carbon. The densities of these materials are not clearly defined as they vary with the microscopic scale-length used. The experimental bulk density (loosely packed material), being a macroscopic property, is normally very low, while the density at the sub-nanometre level as measured by pycnometric methods using He often is

close to that of graphite, $\rho = 2.25$ g cm^{-3}. The scale of the density used for reverse Monte Carlo modelling depends on the configuration box of the model, which has the dimension of a few nanometres. This implies density values in between bulk and graphite and is primarily determined by the number and dimensions of holes in the sample. This complication may be one explanation of why there are only a few reports on nanoporous carbons presenting radial distribution functions, which include estimations of the co-ordination number of the carbon, e.g. [17]. The next step, to derive a three-dimensional structural model, gives additional complications. This is highly desired as there is an interest to derive atomic configurations that can explain properties such as sorption and desorption experiments and are consistent with the experimental structure factor $S(q)$ or radial distribution factor $g(r)$. There are no direct methods to obtain a three-dimensional structure from the structure factor $S(q)$; instead, modelling must be used. One frequently used method for disordered systems is reverse Monte Carlo (RMC) modelling based on the Metropolis algorithm developed by McGreevy and Pusztai [21]. The straightforward but naive description of RMC is that Monte Carlo moves are performed on a large number of carbon atoms placed in a box, and this configuration of atoms is modified to best match the experimental data. The results are structural models that are statistically consistent with the experiment. However, there are an infinite number of atom configurations which can give a reasonable fit to the data using the RMC method, most of which include unrealistic structure fragments. One such fragment frequently obtained during unconstrained RMC simulations of more or less amorphous carbons is a small C-ring fragment that most frequently contains C–C–C angles of 60° [22]. It is therefore necessary to minimize the number of such fragments by controlling which atomic positions are acceptable using various geometric constraints. Of course the starting model is also of major importance. Random models as well as those based on the graphite structure and more complex ones have been used. An important parameter for the starting model is the lower limit in q-range reached by the diffraction data, that influences the density of the structural model. Conventional diffraction data typically end at $q = 0.2$–0.3 Å^{-1}, corresponding to interatomic sizes of ∼20 Å in direct space, but small-angle diffraction techniques such as SANS (small-angle neutron scattering) and SAXS (small-angle x-ray scattering) can be used to reach lower q-values, typically ∼0.02 Å^{-1}. This corresponds to structural features up to 300 Å in size. The lower the q-value reached, the lower the densities of the model as larger pores have to be included in the atomic configuration. The problems of modelling amorphous carbons and different ways to approach them have recently been discussed by Bandosz *et al* [23]. For these reasons there are several problems associated with structural studies of nanoporous carbons using RMC modelling, which need to be taken into account.

An example of RMC modelling using $g(r)$ data based on SAXS combined with conventional XRD (x-ray diffraction) data to obtain an extended q-range is given by Thomson and Gubbins [24] in a structural study of activated mesocarbon micro-beads. Their starting model was based on graphitic plates with size and orientation refined using RMC. They used the following rigid constraints: (i) any given atom can only have two or three neighbours; (ii) all interatomic distances are 1.42 Å; (iii) all bond angles are 120°. The hard constraint with bond angles fixed at 120° solved the problem with unphysical 60° bond angles often occurring in refinement of carbons [22, 25]. Their model density was rather low, 0.97 g cm^{-3} based on the actual carbon density of the sample and in agreement with the q-range of their data. The hard constraint on the C–C–C angle is suitable for graphitic-like carbon while for other types of porous carbons a softer constraint forcing the angle to be around 120° is more appropriate such as in studies of highly porous amorphous carbon made by Pikunic *et al* [26]. In that study which used a random starting model, the distribution of the number of nearest neighbours was allowed to vary around the nominal value of 3. Also here an extended q-range was used,

0.02 to 14.0 $Å^{-1}$, by combining SAXS and XRD data. The densities used were based on Hg porosity measurements and were 1.275 and 1.584 g cm^{-3} for two different samples. In a recent RMC study of glassy carbon V25 using neutron diffraction data starting from a larger q-value on a model based on graphitic layers, the density of graphite was used [27]. In the subsequent RMC modelling using the structure factor $S(q)$, energy-based constraints were used to avoid unphysical structures such as three- and four-member rings. This was achieved by incorporating an environment dependent interaction potential (EDIP) [28] in the refinement.

An alternative widespread method for simulation of disordered structures is molecular dynamics, MD. It has been intensively used to reach a rather complex understanding of the structures of amorphous carbon (a-C) and tetrahedrally bonded amorphous carbon (ta-C) [29, 30]. Although MD calculations clearly show that there is a relation between the density of the amorphous carbon and the sp^3 content, less is known for the low density carbons like those in this study. In these carbons the network is very flexible, leading to many structures very similar in energy. These problems have recently been discussed in a tight binding molecular dynamics study of amorphous carbons with densities from diamond ($\rho = 3.46$ g cm^{-3}) to low density amorphous carbon ($\rho = 1.20$) g cm^{-3} performed by Mathioudakis *et al* [29]. The MD result from the low density carbon is a very disordered structure. The bonding is more or less exclusively sp^2 (66%) and sp^1 (33%) with a significant number of three rings (26%) besides four to seven rings. Thomson and Gubbins [24] mentioned above used a different approach when they refined the orientation and size of rigid carbon based plates using molecular dynamics. The radial distribution function of the resulting model was then used as a test structure for the RMC method. The structural characteristics of the resulting RMC model were in good agreement with those for the starting model from MD, thus validating the RMC method.

In the present study we have performed RMC modelling using neutron powder diffraction data from a number of carbon samples prepared from TiC at $T = 700, 800, 900, 1000$ and 1100 °C. Four different starting models were tested in combination with a soft constraints forcing the C–C–C angles to be around 120° and the co-ordination to be two or three with a certain permitted variance. The correctness of these constraints has been supported by the EELS studies, which strongly show the carbon to have a sp^2/sp^3 ratio close to that found in graphite. The results from RMC modelling are compared with those from low temperature N_2-sorption and HREM studies in order to discuss the structural changes in the carbons as the synthesis temperature increases.

2. Experimental details

The nanoporous carbon materials in this study were made by chlorination of titanium carbide at temperatures between 700 and 1200 °C. During the reaction $TiCl_4$ is leaving the reactor with an excess of chlorine, resulting in a product of pure carbon. A post-treatment of the carbon products in Ar(g) at 1000 °C for 1 h is performed to remove chlorine from the reactor and carbon, after which the samples are cooled down in Ar(g) atmosphere. The reaction can be described as

$$TiC(s) + 2Cl_2(g) \Rightarrow TiCl_4(g) + C(s).$$

A detailed description of the conditions for the synthesis can be found in [5].

High-resolution transmission electron microscopy (HRTEM) studies were made using a transmission electron microscope, JEOL 3010, operated at 300 kV. For these studies, carbon powder was dispersed in n-butanol using an ultrasonic bath and transferred to a copper grid coated by a holey carbon film.

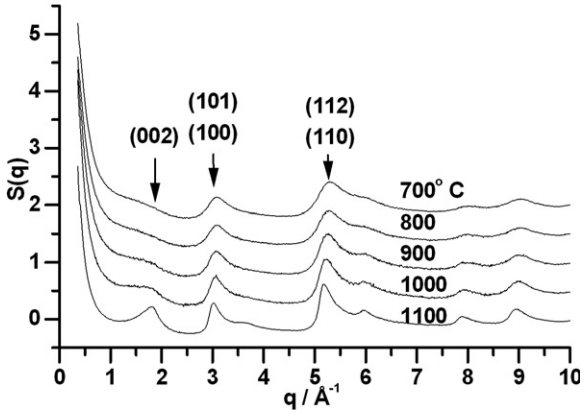

Figure 1. Structure factors of carbons obtained from TiC at 700–1100 °C. The positions of the strongest peaks in crystalline graphite are marked.

The low temperature nitrogen sorption was performed at the boiling point of nitrogen using the surface area and porosity analyser ASAP 2020 (Micrometrics). The specific surface areas of the carbon materials were calculated according to BET theory [31]. (The same range of data was used for all samples.) Pore size distribution calculations were made using the (N_2) original DFT model applying slit pore geometry [32]. The microporous part of the pore volume and the surface area were determined from t-plots. The He-pycnometric densities of the materials are typically close to that of graphite, e.g. 2.1–2.2 g cm^{-3}.

Neutron diffraction data at room temperature for the samples made at 700–1100 °C were measured with the Studsvik liquid and amorphous neutron diffractometer SLAD at NFL [33]. Standard corrections for absorption, multiple scattering, background etc were applied and the data were normalized to a vanadium rod standard to obtain the structure factors shown in figure 1.

2.1. RMC modelling

RMC simulations were used to produce a three-dimensional atomic model of the measured samples. An initial configuration of atom positions is created and random moves of the atoms are performed. During this process the pair distribution function $g^C(r)$ and total structure factor $S^C(q)$ are calculated from the configuration and compared to the experimentally determined functions $g^E(r)$ or $S^E(q)$. Moves that improve the fit to the experimental data are accepted while other moves are accepted only with some small probability. A number of constraints can be applied on the configuration such as a closest approach permitted between atoms and preferred co-ordination numbers. For more details on the RMC technique see [34, 35]. In this work we have used the structure factor $S(q)$ for a q-range of 0.3–10.5 Å^{-1}.

The smallest momentum transfer measured, $\hbar q_{\min}$, will determine an upper limit on the size of any feature that can be modelled, and is on the order of $L/2 = 2\pi/q_{\min}$ where L is the box length. To reproduce the strong peak at low q which reaches down to $q_{\min} = 0.3$ Å^{-1}, the length of the model box must be at least 42 Å, but preferably bigger. Even with a periodic boundary condition of the box the limited size will give rise to oscillations in the calculated structure factor. To minimize the problem with the limited box size a convolution of the measured structure factor in r-space with a step function that is unity for $r \leqslant L/2$ and zero for $r > L/2$ was performed in a standard way. The density of the model was determined

by running a series of Fourier transforms of $S^E(q)$ to $g^E(r)$ with MCGR [19, 20] at different densities and selecting the one giving the best fit to the measured data. (The fit between experimental $S(q)$ and modelled $S(q)$ using MCGR was extremely good and it is difficult to distinguish between the two curves.) The selected density was 0.62 times that of graphite (2.25 g cm^{-3}) or 1.40 g cm^{-3}. (This density did not vary significantly between the different carbons.)

Three different starting models were generated.

(i) The random model (RM), a completely random configuration which consisted of 8000 atoms in a box of dimensions $48.4 \times 48.4 \times 48.4$ Å^3. The atoms were then moved so that all C–C distances were longer than 1.0 Å.

(ii) The separated layer model (SLM), complete graphitic layers which were separated from 3.35 to 5.40 Å to obtain a lower density. (This large separation between the layers can be argued for as the intensity of the 002 reflection is negligible in the samples obtained at 700–1000 °C.) The configuration consisted of 8000 atoms in ten layers.

(iii) The defect layer model (DLM), two models I and II consisting of defect graphitic layers separated to 3.40 Å, which is the separation given by the position of a weak 002 reflection in the $S(q)$ for the carbon produced at 1100 °C (at $q = 1.85$ Å^{-1}). The defects were primarily constructed by arbitrarily removing carbons to obtain the desired density (1.4 g cm^{-3}). To avoid zero- or single-co-ordinated atoms these were identified and manually moved to a position where they had two or three neighbouring atoms.

Using more than one model gives us the possibility to compare the influence of the starting configuration on the final configuration.

The use of the graphene layer structures in the starting structure for the RMC modelling is supported by Raman spectroscopy studies of the samples. The relative intensity ratio of the D and G peaks (I_D/I_G) in these carbons corresponds to L_a values between ~13 and ~16 Å, only slightly below the information limit of the structure factors $S(q)$, and half the size of the RMC modelling box [36]. The L_a values are also very close to those reported by Danishevskii *et al* for similar carbons [37].

A number of constraints were introduced in the RMC modelling. In all starting models the closest approach was 1.0 Å. To avoid zero- or single-co-ordinated atoms, co-ordination constraints for these values were applied (set to zero) for a nearest-neighbour distance of up to 1.6 Å. Above the first peak in $g(r)$, no atoms were allowed between 1.7 and 2.1 Å to avoid small unphysical peaks forming in the radial distribution function. These distances are too long for significant C–C bonding but significantly shorter than the C–C van der Waals distance.

According to the EELS studies we expect to have a large number of sp^2 bonded carbons, that is, a C–C–C triplet angle of 120°. Unrealistic triplets with a 60° angle are easily formed [15, 25] without the use of co-ordination constraints of various kinds as discussed above. To avoid these triplets, an angular constraint was included into the RMC code. Similar angular constraints have been used earlier; see [25, 38]. To do this we included an extra term in the expression for χ^2:

$$\chi^2 = \chi_0^2 + \sum_i [\cos\theta_i - \cos\theta_{\text{pref}}]^2/\sigma$$

where the sum is taken over all triplet angles θ_i in the system, θ_{pref} is the preferred angle, σ is a weight factor and χ_0^2 gives the fit to the experimental data as defined in [21]. With this new constraint set to a preferred triplet angle of 120° it was possible to produce a more realistic configuration of atoms avoiding the unphysical 60° angle.

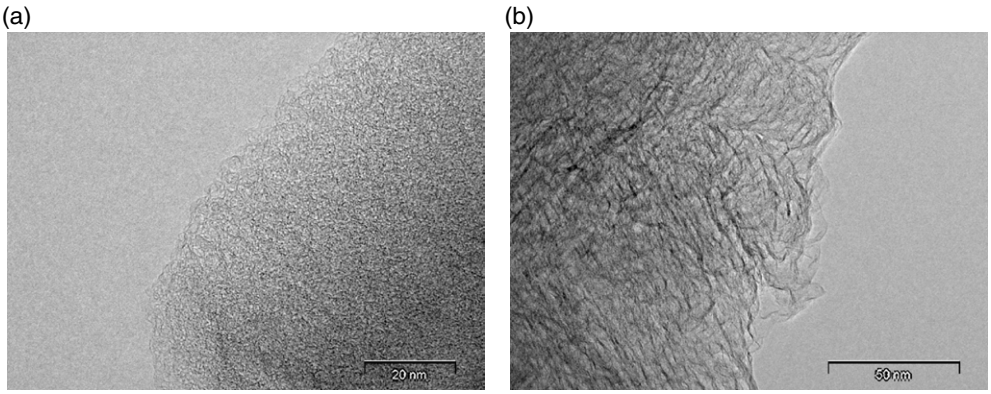

Figure 2. HREM images of nanoporous carbon synthesized at (a) 700 °C and (b) 1100 °C.

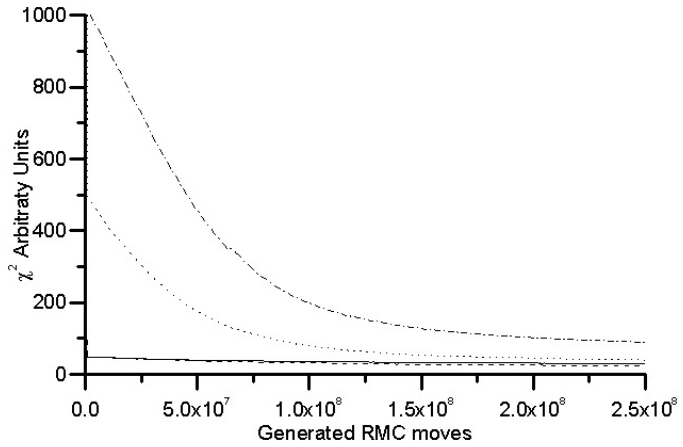

Figure 3. Convergence of the square deviation χ^2 as a function of RMC moves for the 800 °C sample. Dot–dashed line, RM; dotted line, SLM; full line, DLM I; dashed line, DLM II. The small discontinuities are caused by changes in σ during the modelling process.

3. Results and discussion

The experimental $S(q)$ for the neutron diffraction data show all synthesized carbons to be very amorphous although a structural rearrangement has taken place in the 1100 °C sample as seen in figure 1. At 700 °C there is only a very weak graphite interlayer diffraction peak while at 1100 °C a clear 002 peak can be identified with a maximum corresponding to 3.40 Å; however, the structure is still very disordered. These structural differences are clearly observed in the corresponding HREM images shown in figure 2.

The three different starting models had a significant influence on how quickly χ^2 decreased during refinement to reach its final value as shown in figure 3 for the 800 °C carbon. A superior convergence and fit were obtained for the DLM starting models, which is also seen in the observed and calculated $S(q)$ shown in figure 4. The small oscillations seen in the data and fit (also giving rise to the drop of intensity at low q-values) come from a convolution of the experimental $S(q)$ with a step function which is necessary in order to account for the limited box size of the RMC configuration as described previously in section 2.1. The poorest fit

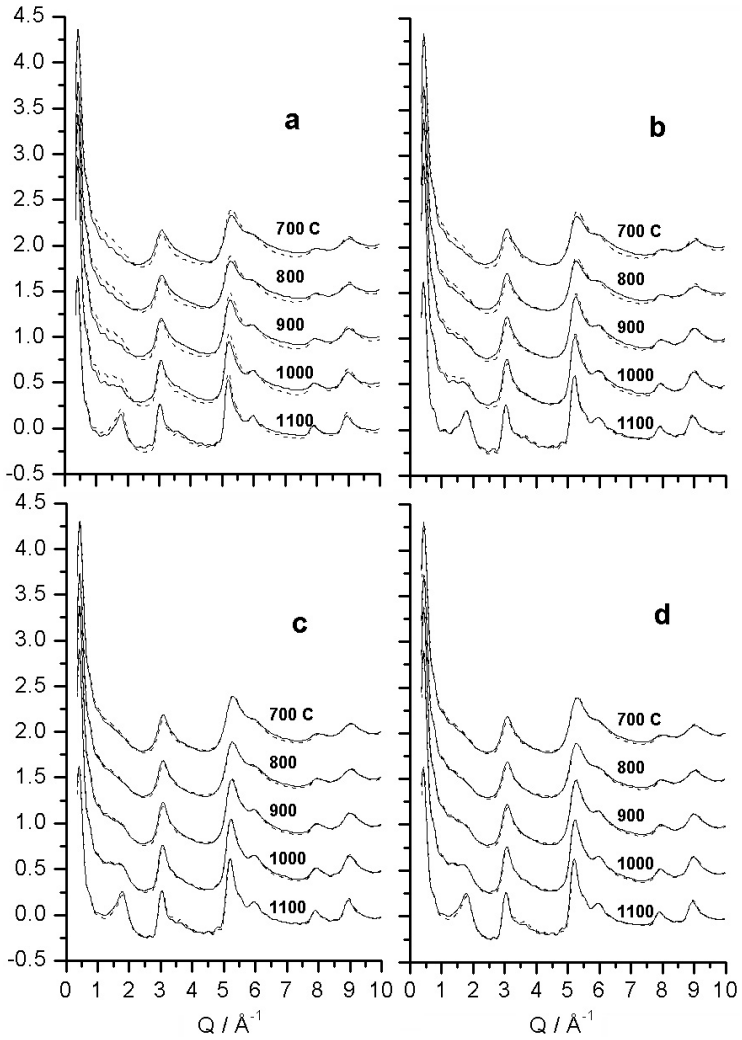

Figure 4. Fits to experimental structure factors (T = 700–1100 °C). The full line is the fitted RMC calculation and the dotted line is the experimental data. The ripples on the structure factors are caused by the convolution of a step function due to the edge effects from the configuration boxes. (a) RM, (b) SLM, (c) DLM I and (d) DLM II.

was found when using random starting models, and therefore these results will not be further discussed in detail.

The distributions of the C–C–C angles for the final atomic configuration are clearly centred around 120° for all temperatures for both the SLM and the DLM starting models as shown in figure 5. This was expected since a rather narrow variance ($\sigma = 0.05 \Rightarrow$ FWHM $\approx 6°$) was allowed. However, it is possible to significantly increase this value without the appearance of C–C–C angles at 60°. For SLM the 60° angles start to appear when $\sigma > 0.5$. The DLM model is less affected by the creation of 60° angles, which only appear with an increased weight on fitting the data.

The radial distribution functions $g(r)$ as calculated from the atomic configurations exhibit the rather broad peaks typical for amorphous carbons as shown in figure 6. The positions of

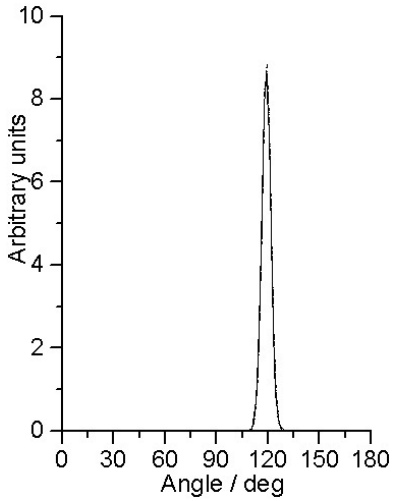

Figure 5. Bond angle distribution for RMC modelling with a defect graphitic start model. All five samples are plotted here but distributions are very similar.

Table 1. Co-ordination number for interatomic distances below 3.3 Å in starting models from above: separate graphite layers, defect graphite layer 1, defect graphite layer 2.

	700 °C	800 °C	900 °C	1000 °C	1100 °C
SLM 1.00–1.80 Å	2.54	2.55	2.56	2.53	2.52
DLM I	2.72	2.71	2.71	2.71	2.71
DLM II	2.78	2.78	2.78	2.78	2.78
SLM 2.00–3.3 Å	12.93	12.91	12.81	12.52	11.22
DLM I	10.06	9.99	9.95	9.62	8.32
DLM II	10.12	10.07	9.99	9.70	8.44

these peaks correspond well to the distances in a single graphite layer shown in figure 7. There are rather well defined peaks up to 5 Å for all temperatures. Outside this range only small peaks can be seen for the 700 °C sample, which increase in size with increasing temperature, indicating larger graphene like structures. The weak peaks/shoulders at 2.10 Å in the 700–1000 °C $S(q)$s are most probably artefacts, although this corresponds to the diagonal distance in a square ring of carbons, which is not likely to exist in these carbons. It should be mentioned that a very similar RDF was obtained using the MCGR program; however, at longer simulation times an increased number of spurious features appeared.

The co-ordination for the three closest co-ordination spheres <3.3 Å is 3:6:3 for a single graphite layer as seen in figure 7. The final atomic configurations, see table 1, reveal a lower number than found in a single graphite layer indicating a large number of double bonded carbons which mainly are positioned at the edges of the graphene flakes. There is also a strong correlation between the co-ordination number and the starting model used which is clearly seen in table 2. For the SLM with CN = 3 in the starting configuration the result is an atomic configuration with the largest number of carbons with CN = 2, while for the two DLM models having slightly different (but lower) average starting CN (2.72 and 2.78) no significant change takes place. There are no clear trends in co-ordination number with the temperature for distances <1.8 Å but for longer distances <3.3 Å, a drop in co-ordination numbers occurs for the 1100 °C sample. A similar result was obtained when using the RDFs obtained from

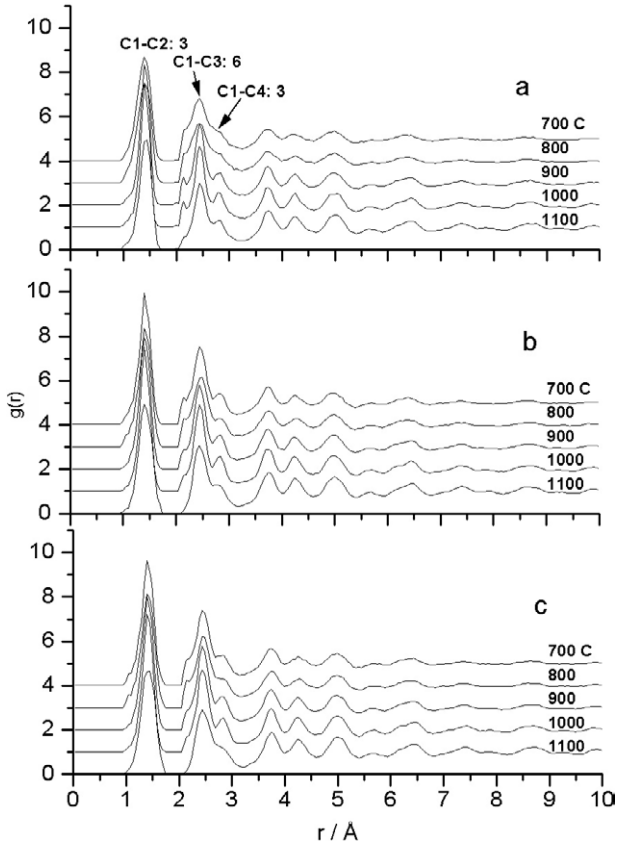

Figure 6. RDF for the different samples: (a) SLM, (b) DLM I, (c) DLM II. The interatomic distances and co-ordination in a single graphite layer are marked.

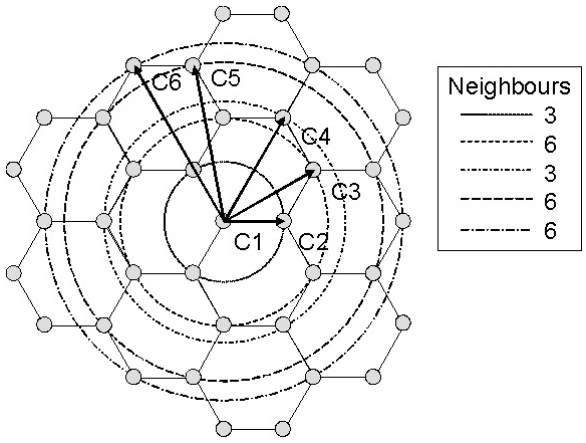

Figure 7. The co-ordination structure of a graphene plane.

the MCGR program. This is somewhat surprising as we expected some systematic increase in co-ordination number with temperature. One reason for the absence of a clear temperature trend could be the problem of choosing the correct density of the models.

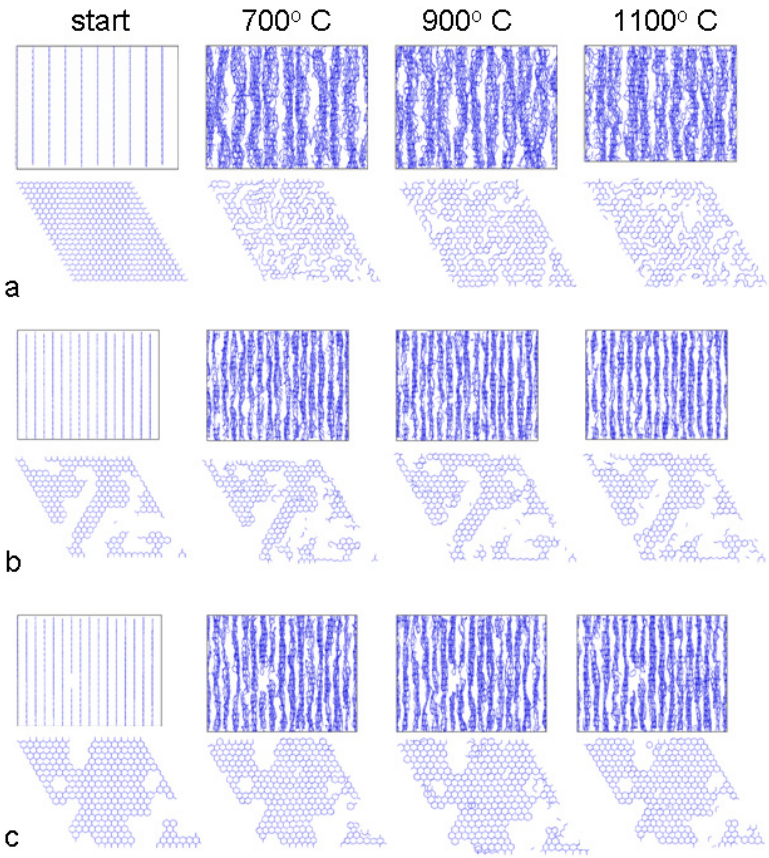

Figure 8. RMC final atom configurations using the three different starting models. Three of the samples are shown ($T = 700$, 900 and 1100 °C) and the start configuration before RMC modelling started. (a) SLM, (b) DLM I and (c) DLM II. The top rows show configurations from the side so that the curvature of the layers can be seen. The bottom rows show one selected layer from corresponding configurations.

(This figure is in colour only in the electronic version)

Table 2. Distribution of neighbours within a radius of 2 Å for three models. Mean values over all five samples are given. Numbers in brackets are the neighbours in the start configurations.

Neighbours	SLM %	DLM I %	DLM II %
0	0.3 ± 0.04 [0]	0.0 ± 0.01 [0]	0.0 ± 0.01 [0.0]
1	0.6 ± 0.05 [0]	1.2 ± 0.01 [1.2]	0.1 ± 0.02 [0.1]
2	43.6 ± 1.5 [0]	26.1 ± 0.1 [25.7]	21.8 ± 0.2 [21.2]
3	55.5 ± 1.5 [100]	72.7 ± 0.1 [73.1]	78.1 ± 0.2 [78.7]

The resulting structure from the SLM and the DLM starting models is shown in figure 8. It should be emphasized that the final atomic configurations are very sensitive to the starting configuration and which constraints have been used during the modelling. Nevertheless, a comparison gives some important information. If a well separated graphite layer (SLM) is the starting model, holes (cavities, pores) are created by moving carbons away from the layers, which lead to a puckering of the graphene layers. Evidence for the creation of the holes is

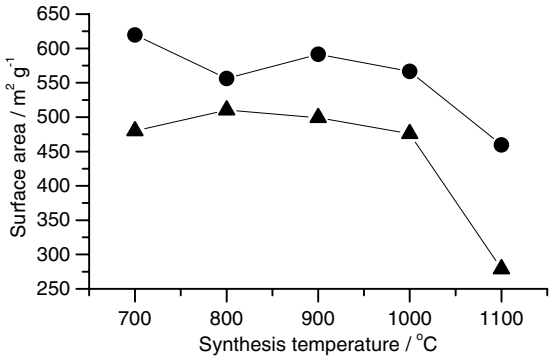

Figure 9. Surface area calculated from the different defect graphite RMC models. Triangles, DLM I; circles, DLM II.

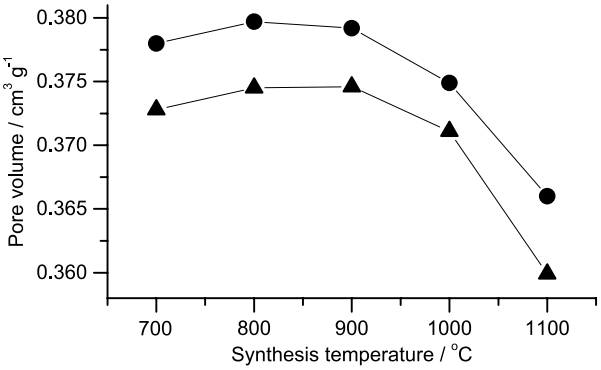

Figure 10. Pore volumes calculated from the different defect graphite RMC models. Triangles, DLM I; circles, DLM II.

the sharp rise in $S(q)$ at low q-values, while the puckering of the graphite layers accounts for the amorphous character of the remaining data. This gives a significant shift in the closest co-ordination number compared with that for a single graphite layer as seen in figure 8. If the holes are present in the starting model the major rearrangement of the atomic configurations is the puckering of the layers to produce a more amorphous structure. Thus there are two tendencies during the modelling: (i) to create cavities in the structure to account for the sharp increase in $S(q)$ at low q; (ii) to create an amorphous structure by puckering and rearrangements of the carbon within a layer to account for the amorphous character of the structure factor, $S(q)$. The presence of vacancies in graphite sheets has recently been confirmed by HRTEM studies [39].

The purpose of these studies is to compare our atomic configurations from the RMC modelling with experimental N_2-sorption results such as surface area, porosity and pore-size distribution. A program based on the methods described in [40] was therefore developed. The surface area, porosity and pore-size distributions from the atomic configurations are shown in figures 9–11, respectively. The volume of micropores, microporous part of the surface area and pore size distribution as determined from the N_2-sorption data in are shown in figures 12–14. A detailed description of the N_2 sorption studies will be published elsewhere [36]. However, the volume of the micropores shown in figure 12 reveals that the microporous part of the pore volume increases with temperature for the 700–900 °C samples. The total surface area

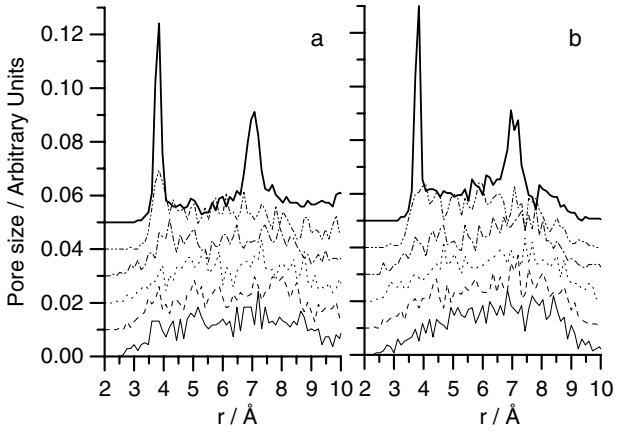

Figure 11. Pore size distribution calculated from different defect graphite RMC models. (a) DLM I and (b) DLM II. From bottom to top: full line 700 °C, dashed 800 °C, dotted 900 °C, dot–dashed 1000 °C, dot–dashed 1100 °C, full thick line start model.

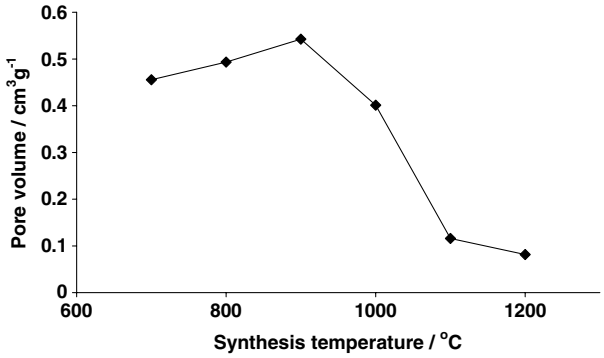

Figure 12. Microporous (V_{micro}) part of the pore volume.

according to BET and its microporous part according to *t*-plots, shown in figure 13, suggests that the increase between 700 and 1000 °C can be attributed to a increasing number of larger pores, while the decrease in pore volume at the higher temperatures mainly has to be addressed to a smaller number of micropores. This picture is even more clearly seen in the pore size distribution shown in figure 14. As the synthesis temperature of the carbon increases the relative number of narrow micropores decreases simultaneously as the volume of pores in the mesoporous region increases.

The general trends for the surface area and pore volumes are the same for the RMC models and the mathematically evaluated N_2-sorption data. For both the RMC modelled pore volume and surface area a clear decrease is observed between the 1000 and 1100 °C atomic configurations. However, the exact values differ between the methods. The main reason is probably the difference in size range, but it should be kept in mind that for RMC the results vary with the starting configurations and constraints used in the modelling. The DLM starting configuration with the lowest porosity resulted in the highest value after RMC modelling. It should be remembered that results from the adsorption isotherms vary depending on which mathematical model is used for the interpretation of the data.

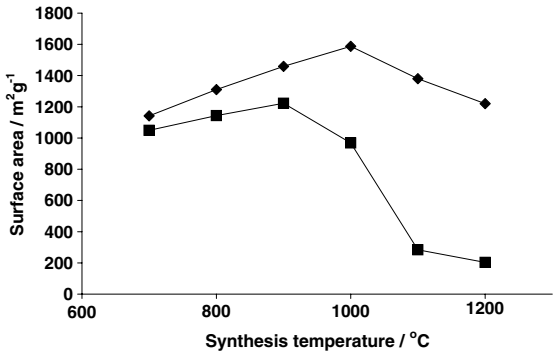

Figure 13. BET surface area (S_{BET}—diamond) and microporous (S_{micro}—squares) part of the surface area (determined from *t*-plots).

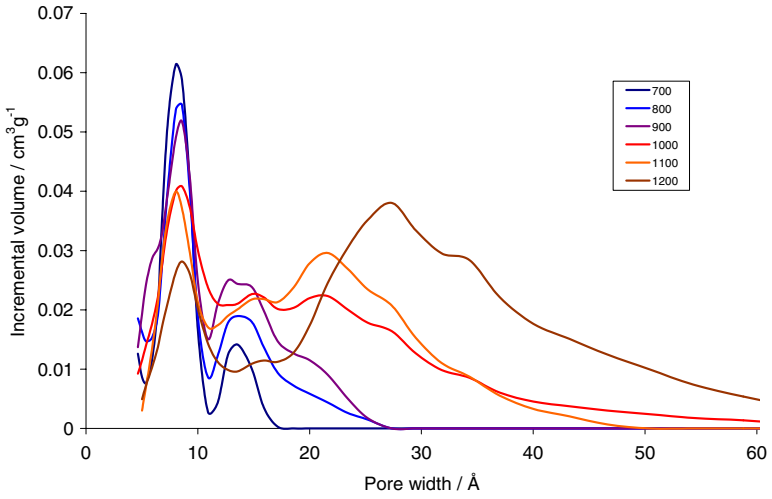

Figure 14. Pore size distributions from sorption data using the DFT model.

The pore size distribution reveals no clear trend with temperature although the 1100 °C data have an indication of a maximum around 4 Å for all starting configurations. This reflects the increased graphitization at 1100 °C. The pore size distribution using the N_2-sorption data gives a different description with a fairly constant pore size maximum at 8 Å, but the total volume decreases with increasing temperature while the number of larger pores increases. This lower maximum should be within the range of the neutron data, but it is not clearly seen in the RMC models. One reason could be the rather small atomic configurations used for the models and lack of low angle data.

A comparison of these results with the same information as determined from N_2-sorption/desorption experiments made on the same samples as the neutron diffraction studies tells us about the feasibility of the neutron diffraction models. However, one has to take in to account the spatial limitations of the data. The N_2-sorption data provide information down to 5 Å, while the neutron diffraction data used here have a practical upper cut-off at approximately 10 Å. Information on larger pore sizes could be obtained by adding low angle scattering data.

A comparison with the carbon structures from our RMC simulations and the MD calculations of low density carbons made by Mathioudakis *et al* [29] reveals some interesting

similarities and differences. As mentioned in the introduction the MD result is a very disordered structure, having a bonding being more or less exclusively sp^2 (66%) and sp^1 (33%) with a significant number of three rings (26%) besides four to seven rings. In fact, the results resemble very much what we get for RMC modelling with very few constraints and a random starting structure. This is not surprising as the MD models are generated by quenching from a high temperature liquid state. In fact, it is more correct to compare with the MD model generated by Thomson and Gubbins [24] using rigid carbon based plates using molecular dynamics. Their structure resembles fairly well the one presented here.

4. Conclusions

These studies show that RMC modelling can be used to study structural changes in nanoporous carbons. However, the results are very dependent on the starting model. Two main trends can be identified in the refined models: (i) a tendency towards the creation of large pores to account for the increasing structure factor $S(q)$ at low q; (ii) a puckering of the graphene sheets to account for the broad peaks. The effect on the modelled atomic configuration is therefore very dependent on the starting configuration used. If the pores are already present in the structure the main change takes place outside the first co-ordination sphere. A detailed analysis of the porosity, pore size distribution and surface areas of the atomic configurations shows that the carbon produced at 700–1000 °C significantly differs from that at 1100 °C mainly due to an increasing graphitization.

Acknowledgments

The authors would like to thank Professor S Csillag and Dr E Coronel for help with the EELS studies. This work has been financed by the Swedish Research Council.

References

[1] Conway B E 1999 Electrochemical supercapacitors *Scientific Fundamentals and Technological Applications* (New York: Kluwer–Academic/Plenum)
[2] Pinnavaia T J and Thorpe M F 1995 *Access in Nanoporous Materials* (New York: Plenum)
[3] Setton R, Bernier P and Lefrant S (ed) 2002 *Carbon Molecules and Material* (London: Taylor and Francis)
[4] Gordeev S K, Kukushkin S A, Osipov A V and Pavlov Y V 2000 *Phys. Solid State* **42** 2314
[5] Leis J, Perkson A, Arulepp M, Nigu P and Svensson G 2002 *Carbon* **40** 1559
[6] Burke A 2000 *J. Power Sources* **91** 37
[7] Gogotsi Y, Nikitin A, Ye H, Zhou W, Fischer J E, Yi B, Foley H C and Barsoum M W 2003 *Nat. Mater.* **2** 591
[8] Perkson A, Leis J, Arulepp M, Käärik M, Urbonaite S and Svensson G 2003 *Carbon* **41** 1729
[9] Franklin R E 1950 *Acta Crystallogr.* **3** 107
[10] Franklin R E 1951 *Acta Crystallogr.* **4** 253
[11] Kravchik A E, Osmakov A S and Avarbe R G 1989 *Zh. Prikl. Khim.* **37** 2430
[12] Oberlin A 1984 *Carbon* **22** 521
[13] Ferrari A C and Robertson J 2000 *Phys. Rev.* B **61** 14095
[14] Harris P J F 2003 Molecular models of porous carbons *Chemistry and Physics of Carbon* vol 28, ed L R Radovic pp 1–39
[15] O'Malley B, Snook I and McCulloch D G 1998 *Phys. Rev.* **57** 14148
[16] Szczygielska A, Burian A, Duber S, Dore J C and Honkimaki V 2001 *J. Alloys Compounds* **328** 231
[17] Burian A, Ratuszna A, Dore J C and Howells S W 1998 *Carbon* **36** 1613
[18] Steytler D C, Dore J C and Wright C J 1983 *Mol. Phys.* **48** 1031
[19] Pusztai L and McGreevy R L 1997 *Physica* B **234–236** 357
[20] Zetterström P and McGreevy R L 2000 *Physica* B **276–278** 187
[21] McGreevy R L and Pusztai L 1988 *Mol. Simul.* **1** 359

[22] Gereben O and Pusztai L 1994 *Phys. Rev.* B **50** 14136
[23] Bandosz T J, Biggs M J, Gubbins K E, Hattori Y, Iiyama T, Kaneko K, Pikunic J and Thomson K T 2003 Molecular models of porous carbons *Chemistry and Physics of Carbon* vol 28, ed L R Radovic, pp 41–228
[24] Thomson K T and Gubbins K E 2000 *Langmuir* **16** 5761
[25] Pikunic J, Pellenq J-M, Thomson K T, Rouzaud J-N, Levitz P and Gubbins K E 2001 *Stud. Surf. Sci. Catal.* **132** 647
[26] Pikunic J, Clinard C, Cohaut N, Gubbins K E, Guet J-M, Pellenq R J-M, Rannou I and Rouzaud J-N 2003 *Langmuir* **19** 8565
[27] Petersén T, Yarovsky I, Snook I, McCulloch D G and Ophetal G 2003 *Carbon* **41** 2403
[28] Marks N 2001 *Phys. Rev.* B **63** 35401
[29] Mathioudakis C, Kopidakis G, Kelires P C, Wang C Z and Ho K M 2004 *Phys. Rev.* B **70** 125202
[30] Marks N A, Cooper N C, McKenzie D R, McCulloch D G, Bath P and Russo S P 2002 *Phys. Rev.* B. **65** 075411
[31] Brunauer S, Emmett P H and Teller E 1938 *J. Am. Chem. Soc.* **60** 309
[32] Oliver J P 1995 *J. Porous Mat.* **2** 9
[33] Wannberg A, Mellergård A, Zetterström P, Delaplane R, Grönros M, Karlsson L-E and McGreevy R L 1999 *J. Neutron Res.* **8** 133
[34] Evrard G and Pusztai L 2005 *J. Phys.: Condens. Matter* **17** S1–13
[35] Keen D A, Tucker M G and Dove M T 2005 *J. Phys.: Condens. Matter* **17** S15–22
[36] Urbonaite S, Svensson G, Csillag S and Coronel E 2005 at press
[37] Danishevskii A M, Smorgonskaya É A, Gordeev S K and Grechinskaya A V 2001 *Phys. Solid State* **43** 137
[38] Tucker M G, Keen D A, Dove M T and Trachenko K 2005 *J. Phys.: Condens. Matter* **17** S67–75
[39] Hashimoto A, Suenaga K, Gloter A, Urita K and Iijima S 2004 *Nature* **430** 870
[40] Thomson T T and Gubbins K E 2000 *Langmuir* **16** 5761